Supplementary Information for "*Heat Generation Behavior of High-Voltage Spinel $LiNi_{0.5}Mn_{1.5}O_4$ Cathodes under Varying Cycling Conditions and Material Configurations*"

Kevin Böhm[a], Aleksandr Kondrakov[b], Torsten Markus[a], and David Henriques[a]

[a]Technische Hochschule Mannheim, Institute for Materials Science and Engineering (IMaSE), Paul-Wittsack-Straße 10, 68163 Mannheim, Germany

[b]BASF SE, Carl-Bosch-Straße 38, 67056 Ludwigshafen, Germany

Corresponding author: `k.boehm@th-mannheim.de`

Additional contact: `d.henriques@th-mannheim.de`

1 Additional Figures

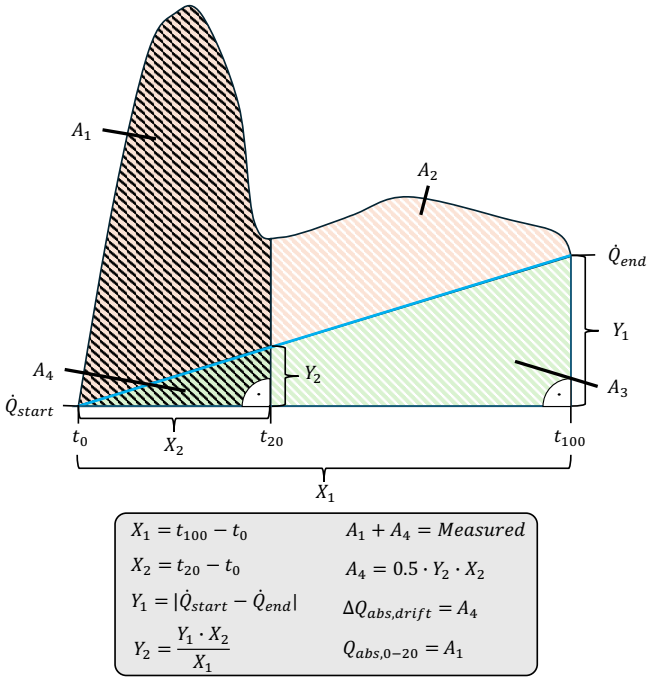

Figure S1: Schematic illustration of the geometrical drift-correction procedure used to determine partial heat-release contributions from calorimetric data. The sketch represents a typical heat-flux profile during the charge of an LNMO half-cell. $\dot{Q}_{\mathrm{start}}$ and $\dot{Q}_{\mathrm{end}}$ indicate the baseline heat-flux level at the beginning and end of the charge step, respectively. The times t_0, t_{20}, and t_{100} correspond to the moments at which 0%, 20%, and 100% $\mathrm{SoC_c}$ are reached. The blue line denotes the linear integration baseline used by Proteus, yielding the total integrated heat $A_1 + A_2$. To isolate the partial heat between 0–20% SoC, the triangular drift-correction area $A_4 = 0.5 \cdot Y_2 \cdot X_2$ is calculated. Subtracting A_4 from the measured value $(A_1 + A_4)$ gives the corrected partial heat A_1. Thus, A_4 represents the drift correction and A_1 the absolute heat released in the 0–20% SoC range. The same correction procedure is applied analogously for discharge.

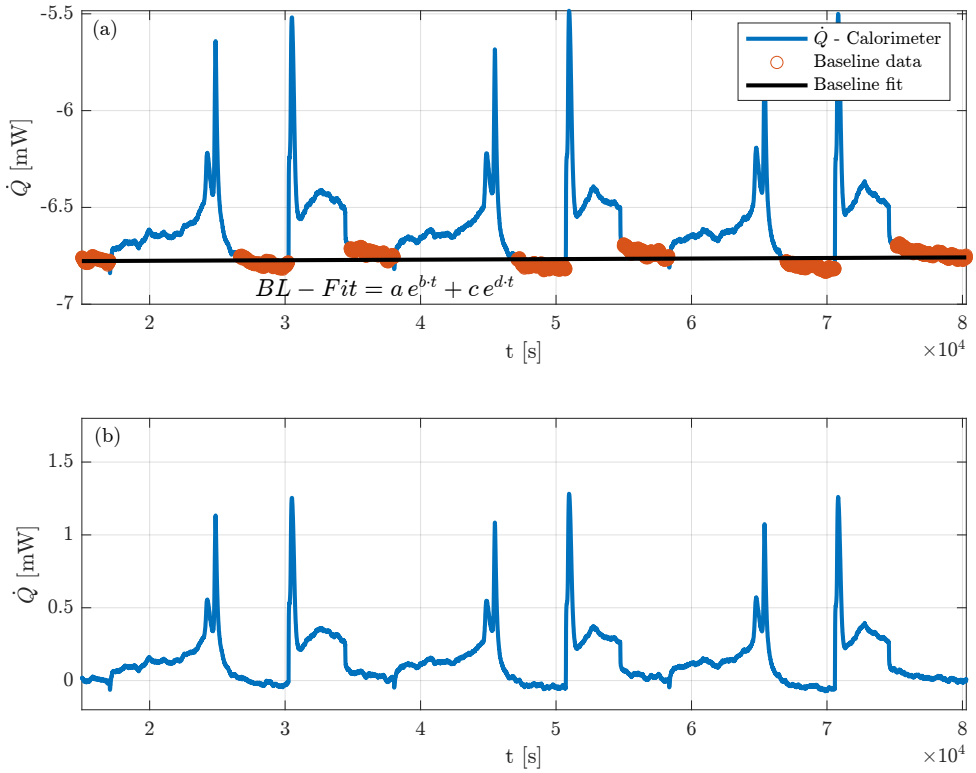

Figure S2: (a) Raw calorimeter heat-flux data (blue) together with the data points used for the baseline fit (orange), corresponding to periods without heat flux due to a current flow. The black curve represents the baseline fit, modeled as a second-order exponential function. The fit was performed individually for each cell using MATLAB's `fit` function with the Levenberg–Marquardt algorithm. (b) Resulting heat-flux signal after subtraction of the fitted baseline from the raw data.

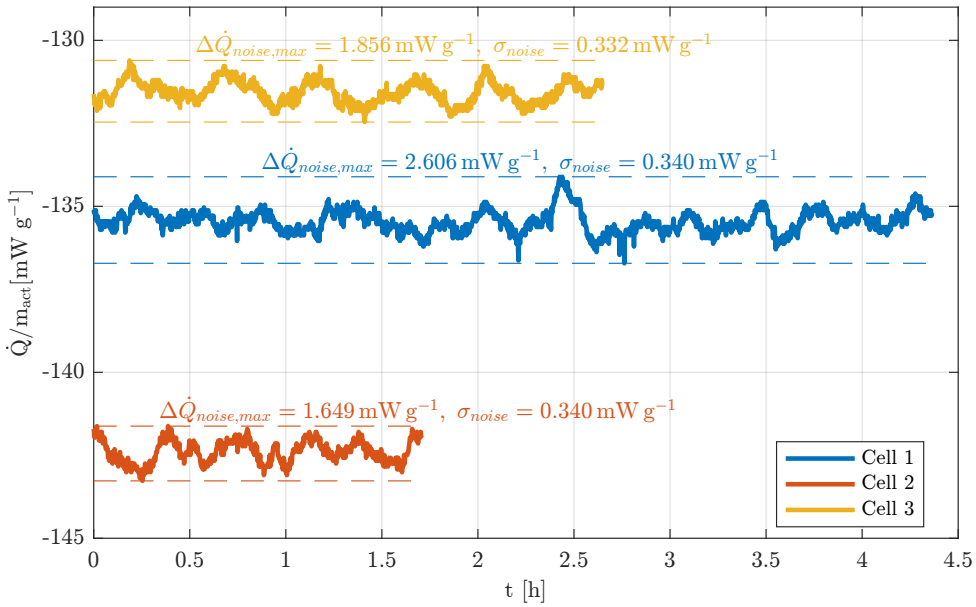

Figure S3: Calorimeter baseline heat-flux signals of cells 1–3 recorded after completion of the current-variation sequence, during periods without applied current. The different temporal lengths of the traces arise from cell-dependent termination times, but each baseline segment was recorded for at least 1.5 h. Across all three cells, a maximum standard deviation of $\sigma_{noise} = 0.35\,\mathrm{mW\,g^{-1}}$ and a maximum peak-to-peak variation of $\Delta\dot{Q}_{noise,max} = 2.61\,\mathrm{mW\,g^{-1}}$ were observed, representing the upper bounds of the calorimeter noise determined in this study.

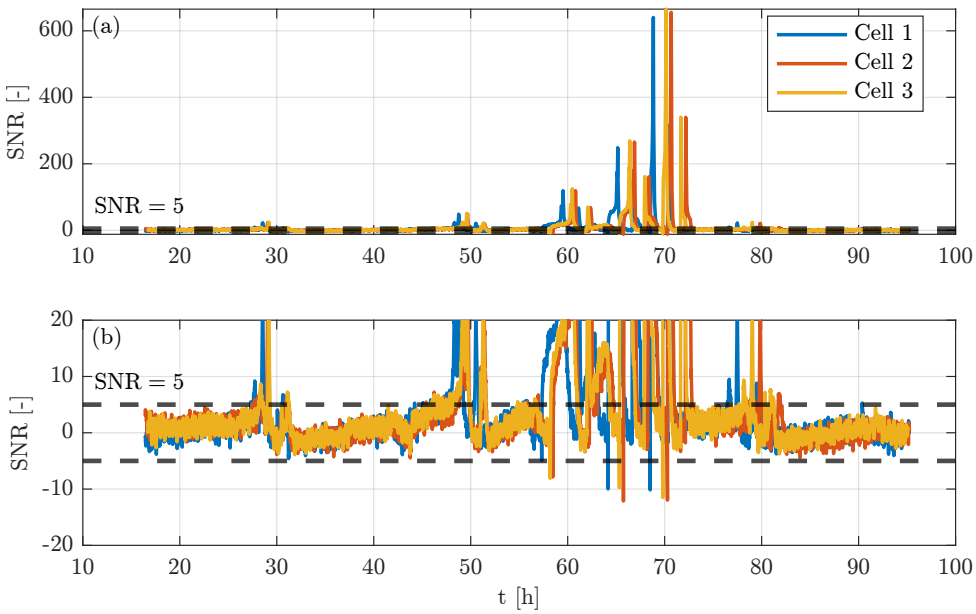

Figure S4: Signal-to-noise ratio (SNR) of the calorimetric heat-flux signals of cells 1–3 during the current-variation test series, calculated using a baseline noise of $\sigma_{noise} = 0.35\,\mathrm{mW\,g^{-1}}$. For all measurements, the dominant heat-flux peaks exceed the threshold of SNR = 5, indicating reliable peak detectability. For the low C-rates of 0.1 and $0.2\,\mathrm{h^{-1}}$, however, most of the signal remains below SNR = 5, which is why no heat-flux integration is performed for these steps; only the peak values carry sufficient significance. Subfigure (a) shows the full SNR traces, while subfigure (b) provides a magnified view of the range $-20 \leq \mathrm{SNR} \leq 20$. For a detailed mapping of the signal progression to the applied current profile, see Fig. S5.

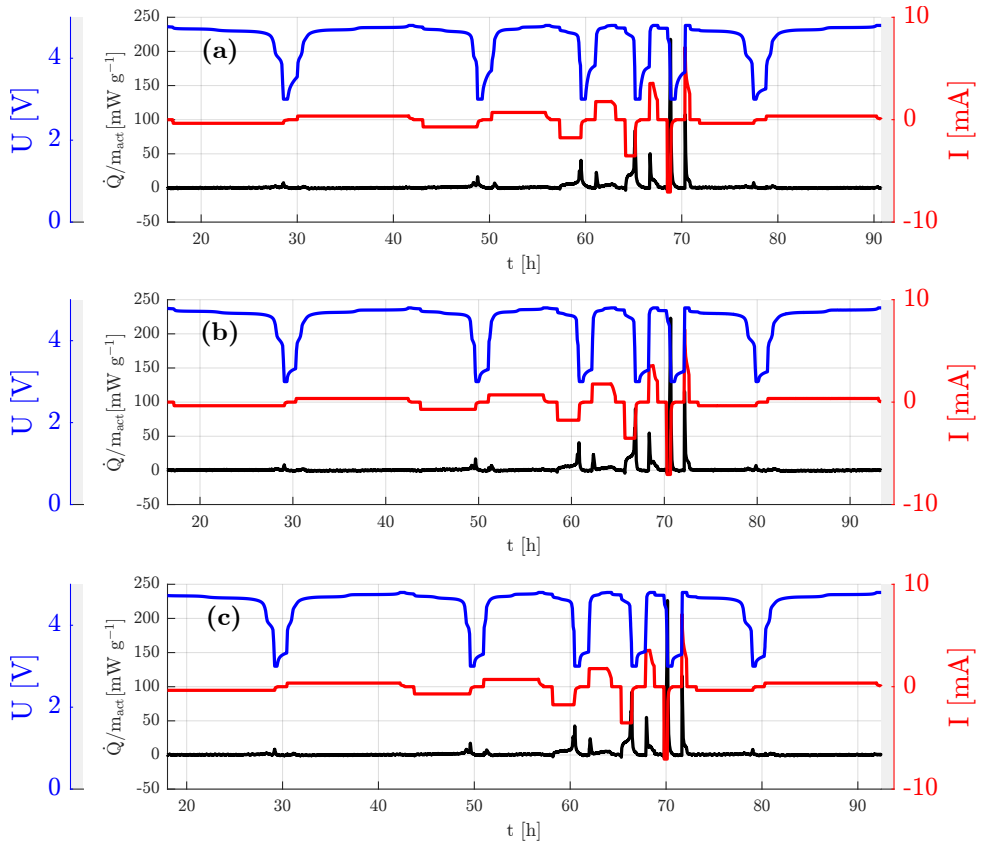

Figure S5: Current, voltage, and heat flux profiles over time for cells 1, 2, and 3 during the current variation test series. Subfigure (a) shows the data for cell 1, (b) for cell 2, and (c) for cell 3.

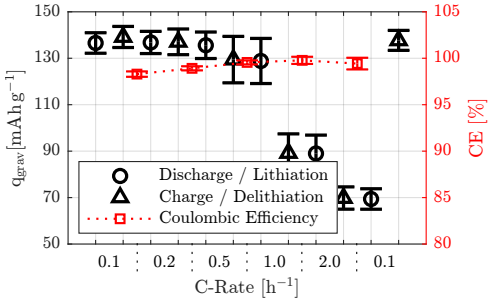

Figure S6: Coulombic Efficiencies (CE) for each charge/discharge pair as a function of the applied charge. Due to the measurement protocol, charging and discharging were conducted at different current rates. As a result, the first discharge and final charge are not included in the CE calculation.

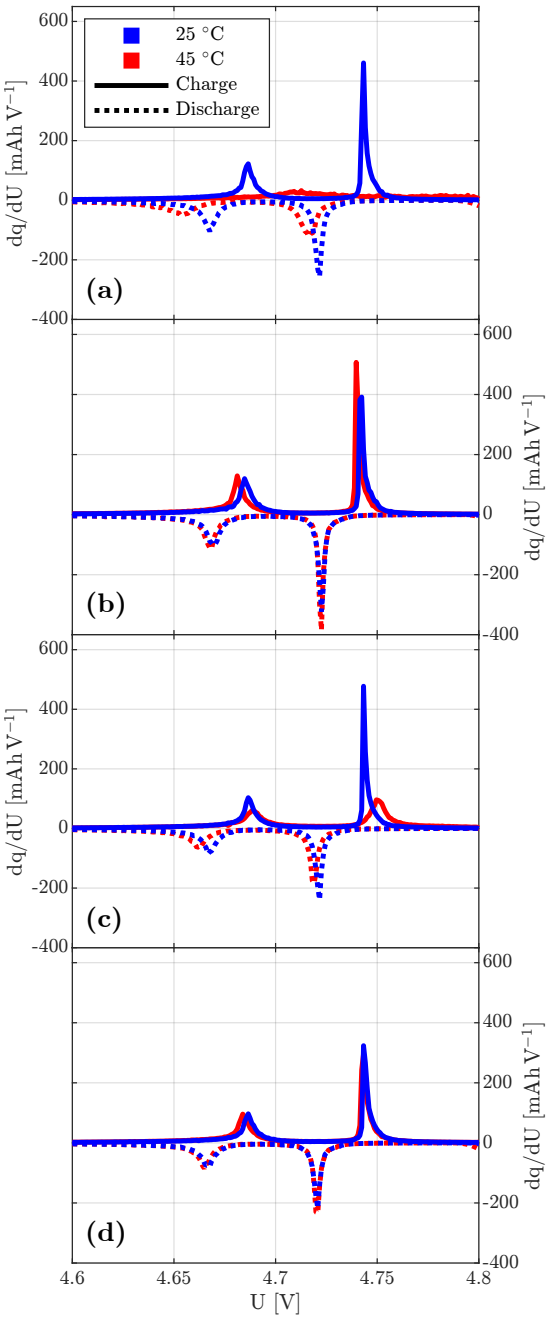

(A) The subfigure assignments are as follows: (a) C_IE_S (cells: 7, 19), (b) C_IE_I (cells: 4, 16), (c) C_SE_S (cells: 13, 25), (d) C_SE_I (cells: 10, 22).

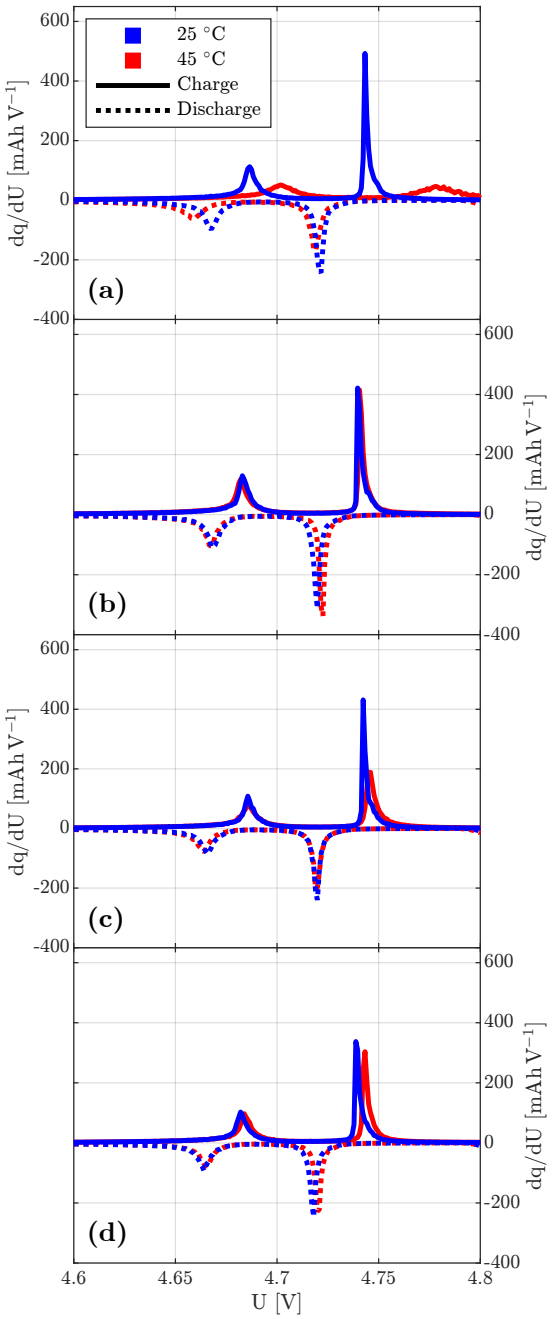

(B) The subfigure assignments are as follows: (a) C_IE_S (cells: 9, 21), (b) C_IE_I (cells: 6, 18), (c) C_SE_S (cells: 15, 27), (d) C_SE_I (cells: 12, 24).

Figure S7: ICA measurements of the remaining cells for all cathode–electrolyte combinations not shown in the main part of the publication. For clarity, only one representative cell per material combination and temperature is displayed in each subfigure. The voltage range is limited to 4.6–4.8 V to exclude the relatively small Mn redox peak around 4 V.

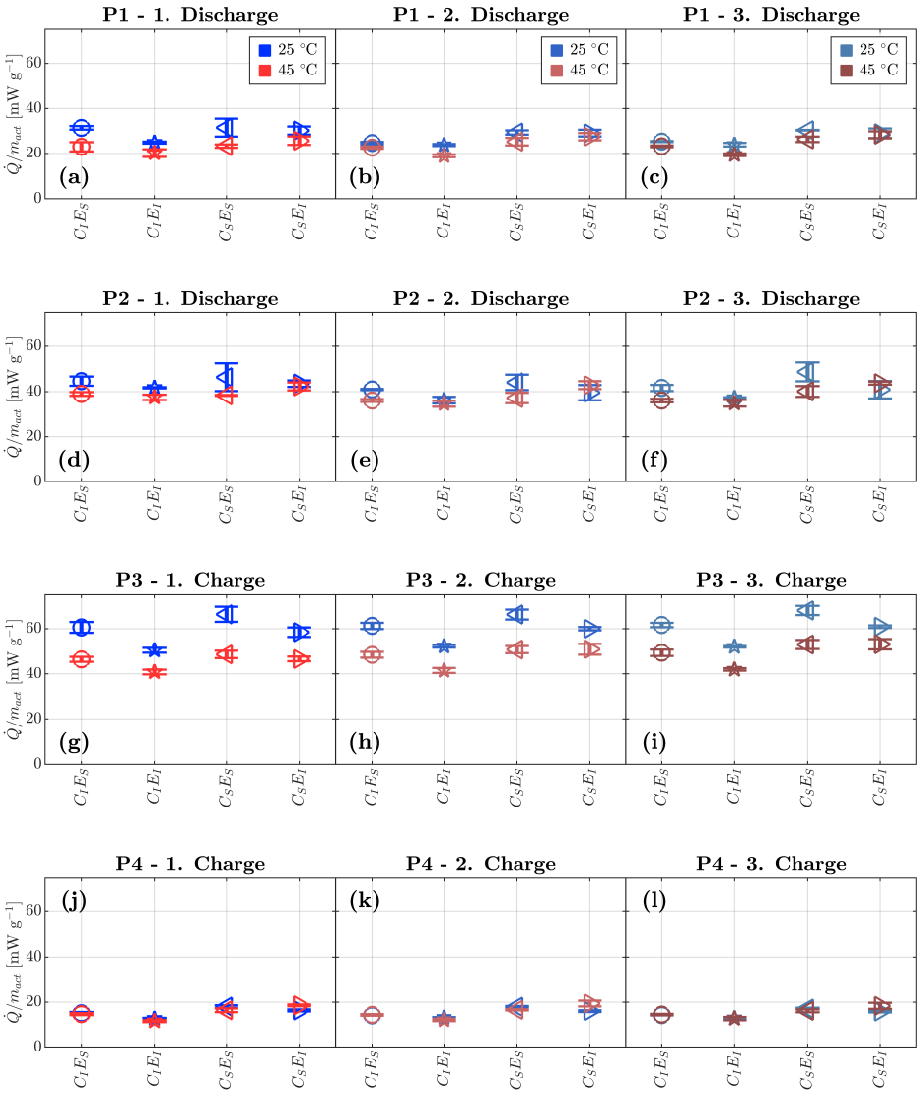

Figure S8: Maximum values of the heat flow peaks P1 (a–c), P2 (d–f), P3 (g–i), and P4 (j–l) for all four material configurations at 25 °C and 45 °C. Each subplot displays the evolution across the three calorimetric cycles.

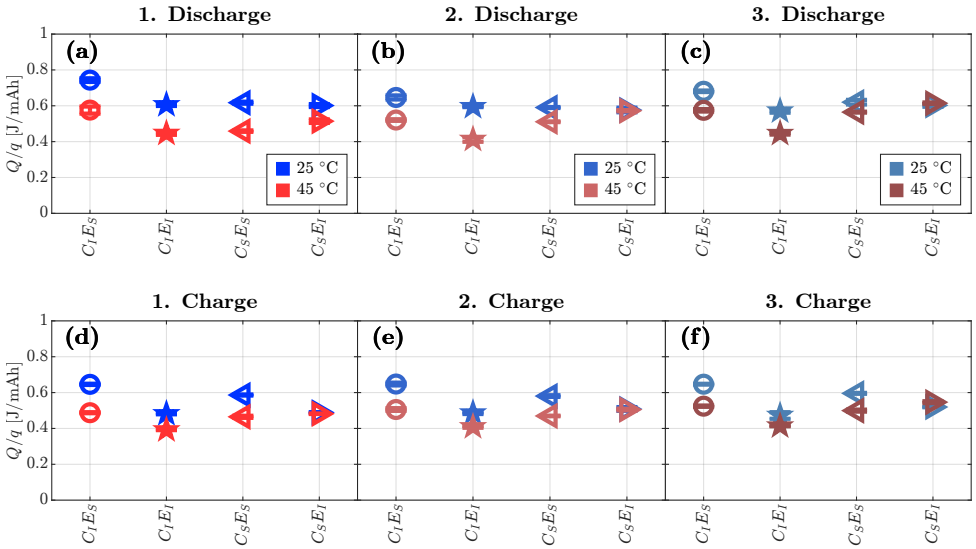

Figure S9: Normalized heat generation during discharge (a–c) and charge (d–f) for all four material configurations at 25 °C and 45 °C. Each subplot shows the evolution over the three calorimetric cycles.

2 Additional Tables

Table S1: Root-mean-square error ($RMSE_{Fit}$) of the baseline fit for each cell, calculated from the deviation between the fitted baseline and the baseline data points shown in the previous figure. The $RMSE_{Fit}$ is normalized to the active-material mass; the small mass-determination uncertainties (± 0.02 mg for C_S and ± 0.04 mg for C_I) were neglected. For completeness, the maximum absolute deviation ($MaxAbs_{Fit}$) is also reported. The total cell-level uncertainty σ_{Cell} combines RMSE and the calorimeter noise ($\sigma_{noise} = 0.35$ mW g^{-1}). The group-level uncertainty σ_{Group} is obtained by Gaussian error propagation of the three cells within each group. The dominant contributor to σ_{Cell} is an uneven baseline, which increases the RMSE.

Cell	$RMSE_{Fit}$ [mW g^{-1}]	$MaxAbs_{Fit}$ [mW g^{-1}]	σ_{Cell} [mW g^{-1}]	σ_{Group} [mW g^{-1}]
1	0.41	1.76	0.54	
2	0.51	1.55	0.62	0.34
3	0.49	1.49	0.61	
4	0.63	3.68	0.73	
5	0.54	1.96	0.65	0.39
6	0.52	1.46	0.63	
7	0.63	2.78	0.73	
8	0.61	1.83	0.71	0.39
9	0.46	1.69	0.58	
10	0.96	2.68	1.03	
11	0.95	2.38	1.02	0.63
12	1.14	2.57	1.20	
13	1.44	3.12	1.49	
14	1.26	2.99	1.31	0.74
15	0.91	2.27	0.98	
16	3.15	6.22	3.17	
17	3.05	5.93	3.08	1.78
18	2.95	5.34	2.98	
19	2.31	5.68	2.34	
20	2.44	4.89	2.47	1.39
21	2.38	5.24	2.41	
22	1.17	3.35	1.23	
23	1.01	2.99	1.07	0.64
24	0.91	3.53	0.98	
25	0.73	2.07	0.81	
26	0.85	1.86	0.92	0.52
27	0.89	2.52	0.96	

Table S2: Absolute heat release of each C_IE_I cell measured at 25 °C. The calorimeter uncertainty, determined from calibration, is estimated as $\pm 1\,J\,g^{-1}$. The geometrical drift correction $\Delta Q_{abs,drift}$ is obtained from a linear-extrapolation approach; its associated uncertainty is approximated as $\Delta Q_{abs,drift}/2$.

Cell	Cycle	Phase	$Q_{abs,0-100}$ [J g^{-1}]	$Q_{abs,0-20}$ [J g^{-1}]	$\Delta Q_{abs,drift}$ [J g^{-1}]
4	1	Discharge	76.79 ± 1.00	44.13± 1.04	0.03
		Charge	45.55 ± 1.00	18.49± 1.00	0.04
	2	Discharge	59.18 ± 1.00	33.71± 1.04	0.28
		Charge	46.20 ± 1.00	19.36± 1.00	0.04
	3	Discharge	58.01 ± 1.00	32.37± 1.00	0.10
		Charge	47.46 ± 1.00	19.37± 1.00	0.02
5	1	Discharge	64.37 ± 1.00	34.48± 1.28	0.79
		Charge	45.42 ± 1.00	18.73± 1.00	0.03
	2	Discharge	56.14 ± 1.00	30.54± 1.00	0.01
		Charge	48.58 ± 1.00	19.95± 1.00	0.02
	3	Discharge	56.74 ± 1.00	31.35± 1.01	0.13
		Charge	47.75 ± 1.00	19.79± 1.00	0.03
6	1	Discharge	69.37 ± 1.00	36.05± 1.06	0.37
		Charge	48.21 ± 1.00	20.21± 1.00	0.05
	2	Discharge	55.72 ± 1.00	28.85± 1.00	0.03
		Charge	48.04 ± 1.00	20.53± 1.00	0.03
	3	Discharge	53.12 ± 1.00	28.65± 1.01	0.13
		Charge	47.28 ± 1.00	20.48± 1.00	0.05

Table S3: Absolute heat release of each C_IE_I cell measured at 45 °C. The calorimeter uncertainty, determined from calibration, is estimated as $\pm 1\,J\,g^{-1}$. The geometrical drift correction $\Delta Q_{abs,drift}$ is obtained from a linear-extrapolation approach; its associated uncertainty is approximated as $\Delta Q_{abs,drift}/2$.

Cell	Cycle	Phase	$Q_{abs,0-100}$ [J g^{-1}]	$Q_{abs,0-20}$ [J g^{-1}]	$\Delta Q_{abs,drift}$ [J g^{-1}]
16	1	Discharge	62.24 ± 1.00	35.30 ± 1.00	0.00
		Charge	47.70 ± 1.00	16.37 ± 1.00	0.18
	2	Discharge	47.15 ± 1.00	25.40 ± 1.00	0.04
		Charge	44.64 ± 1.00	16.71 ± 1.00	0.15
	3	Discharge	48.48 ± 1.00	25.02 ± 1.00	0.18
		Charge	44.41 ± 1.00	17.30 ± 1.01	0.28
17	1	Discharge	51.81 ± 1.00	27.19 ± 1.03	0.51
		Charge	49.47 ± 1.00	16.67 ± 1.00	0.17
	2	Discharge	52.48 ± 1.00	27.87 ± 1.13	1.04
		Charge	48.97 ± 1.00	17.65 ± 1.01	0.28
	3	Discharge	50.48 ± 1.00	26.74 ± 1.06	0.72
		Charge	48.77 ± 1.00	17.34 ± 1.01	0.33
18	1	Discharge	68.57 ± 1.00	38.98 ± 1.24	1.47
		Charge	45.61 ± 1.00	16.19 ± 1.00	0.11
	2	Discharge	49.02 ± 1.00	26.11 ± 1.00	0.02
		Charge	47.79 ± 1.00	17.61 ± 1.01	0.20
	3	Discharge	51.85 ± 1.00	26.92 ± 1.00	0.11
		Charge	46.10 ± 1.00	17.72 ± 1.01	0.26

Table S4: Absolute heat release for $C_I E_I$ during the first three cycles at 25 °C and 45 °C. Values are given in $J\,g^{-1}$ and correspond to the integrated heat over the 0–20 % and 0–100 % $SoC_{d/c}$ ranges. The table summarizes the mean values from Tables S2 and S3, with the error bars representing the estimated standard deviation (ESD) of the three independently assembled cells for each temperature and phase.

Temp.	Phase	Cycle 1		Cycle 2		Cycle 3	
		0–20%	0–100%	0–20%	0–100%	0–20%	0–100%
25 °C	Discharge	38.22 ± 5.18	70.18 ± 6.25	31.03 ± 2.47	57.01 ± 1.89	30.79 ± 1.94	55.96 ± 2.53
	Charge	19.14 ± 0.93	46.39 ± 1.57	19.94 ± 0.59	47.61 ± 1.25	19.88 ± 0.56	47.50 ± 0.24
45 °C	Discharge	33.82 ± 6.03	60.87 ± 8.47	26.46 ± 1.27	49.55 ± 2.70	26.23 ± 1.04	50.27 ± 1.70
	Charge	16.41 ± 0.24	47.60 ± 1.94	17.32 ± 0.53	47.13 ± 2.24	17.45 ± 0.23	46.43 ± 2.20